Pharm Res (2012) 29:1020–1032
DOI 10.1007/s11095-011-0644-x

RESEARCH PAPER

Origin of Two Modes of Non-isothermal Crystallization of Glasses Produced by Milling

Sayantan Chattoraj • Chandan Bhugra • Chitra Telang • Li Zhong • Zeren Wang • Changquan Calvin Sun

Received: 18 September 2011 / Accepted: 5 December 2011 / Published online: 16 December 2011

ABSTRACT

Purpose To mechanistically explain the origin of two distinct non-isothermal crystallization modes, single-peak (unimodal) and two-peak (bimodal), of organic glasses.

Methods Glasses of ten organic molecules were prepared by melt-quenching and cryogenic milling of crystals. Non-isothermal crystallization of glasses was monitored using differential scanning calorimetry and powder X-ray diffractometry.

Results The non-isothermal crystallization of glass, generated by milling, is either unimodal or bimodal, while that of melt-quenched glass without being milled is always unimodal. The mode of crystallization of amorphous phase depends on the relative position of the crystallization onset (T_c) with respect to glass transition temperature (T_g), and can be explained by a surface crystallization model. Bimodal crystallization event is observed when T_c is below or near T_g, due to the fast crystallization onset at milled glass surfaces. Unimodal crystallization is observed when T_c is well above T_g. We have verified this model by intentionally inducing flip between the two crystallization modes for several compounds through manipulating glass surface area and T_c.

Conclusions The two modes of crystallization of organic glasses is a result of the combined effects of faster surface crystallization and variation in specific surface area by milling.

Electronic supplementary material The online version of this article (doi:10.1007/s11095-011-0644-x) contains supplementary material, which is available to authorized users.

S. Chattoraj • C. C. Sun (✉)
Pharmaceutical Materials Science & Engineering Laboratory
Department of Pharmaceutics, University of Minnesota
9-127B Weaver-Densford Hall, 308 Harvard Street S.E.
Minneapolis, Minneapolis 55455, USA
e-mail: sunx0053@yahoo.com

C. C. Sun
e-mail: sunx0053@umn.edu

C. Bhugra • C. Telang • L. Zhong • Z. Wang
Pharmaceutical Development
Boehringer-Ingelheim Pharmaceuticals Inc.
Ridgefield, Connecticut, USA

KEY WORDS amorphous · bimodal · crystallization onset · glass transition · kinetic flip · surface crystallization · unimodal

INTRODUCTION

The crystallization of glasses is a topic of considerable interest to diverse research fields such as pharmaceuticals (1,2), food sciences (3,4), biochemicals (5) and inorganic material sciences (6–8). Amorphous glasses can be generated either by evading crystallization through quenching of melts, vapor deposition, and freeze drying (1,2), or by mechanical activation of crystalline solids through processes such as milling (9–12), which cause lattice disruption due to accumulation of crystal dislocations resulting from mechanical stress (13). Irrespective of the route of amorphous generation, the amorphous phase of a solid lacks the three-dimensional long range molecular order characteristic of crystals and possesses higher free energy compared to corresponding crystalline states (1,14,15). As a consequence of the higher free energy, amorphous solids are thermodynamically unstable and tend to reorder into a crystalline state (1,16). The physical instability of amorphous solids and their crystallization tendency are of particular importance in drug product development (17–19).

The crystallization during heating of a glass usually emerges as a well-defined single exothermic event in DSC, *i.e.*, unimodal crystallization. However, two distinct exotherms or bimodal events have also been observed, especially during heating of amorphous phase generated through mechanical milling (20,21). Currently, there are different views in the literature regarding the possible physical origin of the appearance of bimodal exotherms. In one view, the bimodal exotherms was attributed to reordering of a milling-induced high energy mesophase (or a defective crystalline state), which is a phase thermodynamically distinct from the true amorphous glass (20,22). Others suggested that the phenomenon may be a result of nuclei-induced glass

surface crystallization followed by crystallization of bulk and amorphous particles free from crystal nuclei (23). In addition, bimodal crystallization of melt-quenched D-mannitol (24) and nifedipine (25) glasses have been attributed to crystallization into two different polymorphs.

It appears that, despite considerable efforts in recent years, the physical basis of the bimodal crystallization phenomenon remains elusive. This hinders the proper understanding of the nature of the instability of organic glasses displaying such a phenomenon and the development of effective strategies to stabilize them. In this work, we describe a model that can explain both the unimodal and bimodal crystallization behaviors of glasses, taking into consideration the relative positions of their crystallization and glass transition temperatures.

MATERIALS AND METHODS

Materials

A total of 10 crystalline drugs were selected as model compounds for this study (Table I). Model compounds were selected on the basis of properties commonly thought to influence the amorphization tendency of crystals, such as the melting temperature and enthalpy of fusion (crystal lattice stability), and glass transition temperature (glass stability). All model compounds were used as received for amorphous preparation, and subsequent calorimetric and X-ray diffraction studies.

Preparation of Amorphous Phase

Amorphous glass for each model compound was prepared by cryogenic milling of crystals and quenching of melts. For cryomilling, approximately 2 g of crystalline powder was milled in a polycarbonate tube submerged in liquid nitrogen bath (6750 Freezer Mill, SPEX CertiPrep, Metuchen, NJ). In this technique, a sample is milled when a magnetically-driven cylindrical stainless-steel milling bar impacts two stainless-steel lids of a polycarbonate tube within which the sample is enclosed. Before milling, the whole milling assembly was pre-cooled in liquid nitrogen (~77 K) for 2 min. Milling was conducted at a rate of 10 impacts per second. A 2 min cooling period was employed after every 2 min of milling. Samples were withdrawn inside a glove box under a dry nitrogen purge at various time points during milling, and stored in a desiccator containing anhydrous calcium sulfate (Dreirite®, W.A. Hammond Dreirite Co. Ltd., OH). Thermal and X-ray characterization on freshly milled samples were performed typically within 5–10 min after sample withdrawal.

Amorphous glasses were also prepared by *ex situ* melt-quenching. Samples were melted in aluminum pans inside a glove box purged with dry nitrogen. Care was taken to ensure complete melting of the powders while avoiding decomposition of samples. Once the sample melted, it was quenched by placing the sample pan on a steel surface (~10°C) inside the glove box. This melt-quenching technique was suitable for preparing amorphous phase for all compounds in this study.

Non-isothermal Crystallization Studies

Crystallization studies were done using a differential scanning calorimeter (DSC, either Q1000 or Q2000, TA Instruments, New Castle, DE) equipped with a refrigerated cooling system. The DSC cell was purged with nitrogen at a rate of 50 mL/min. The baseline of DSC was initially calibrated using an empty DSC cell, followed by placing

Table I Information on Crystal Forms of APIs Milled, Melting Points, Enthalpies of Fusion and Glass Transition Temperatures (T_g). Reported T_g Values are from Reversing C_p Signal of MDSC. Other Parameters have been Obtained at a DSC Heating Rate of 10°C/min. Standard Deviations are for Three DSC Measurements Using Independent Samples

Model compound	Form milled	Melting point (°C)	Enthalpy of fusion (J/g)	T_g (°C)	Supplier
Dipyridamole (DPD)	Form I	161.5 ± 0.13	65.4 ± 2.2	40.2 ± 0.4	Aldrich
Ketoconazole (KNZ)	NA[a]	145.9 ± 0.16	102.5 ± 2.1	42.4 ± 0.3	PHHA Assoc.
Indomethacin (IMC)	Form γ	160.2 ± 0.69	109.1 ± 1.2	46.2 ± 0.3	Sigma-Aldrich
Sulfamethazine (SMT)	Form I	196.2 ± 0.33	111.9 ± 2.1	74.3 ± 0.3	AK Scientific
Terfenadine (TFD)	Form I	151.0 ± 0.25	109.8 ± 0.6	58.6 ± 0.3	Sigma-Aldrich
Felodipine (FLD)	Form I	140.5 ± 0.75	74.5 ± 1.4	46.9 ± 0.2	Aldrich
Sulfamerazine (SMZ)	Form I	235.9 ± 0.73	149.4 ± 2.3	62.5 ± 3.1	Sigma-Aldrich
Piroxicam (PRX)	Form β	200.6 ± 0.37	118.2 ± 3.0	63.0 ± 0.2	Sigma
Griseofulvin (GRF)	NA[a]	219.6 ± 0.42	111.8 ± 1.2	91.3 ± 0.1	Sigma-Aldrich
Hydrochlorothiazide (HCT)	Form I	267.6 ± 0.19	97.2 ± 2.1	118.9 ± 1.1	Sigma-Aldrich

[a] No known polymorph.

sapphire discs, without pans, directly on the reference and sample positions. The temperature and enthalpy calibrations were done using indium. Hermetically sealed aluminum pans without pinholes were used for all studies. To enhance thermal contact with samples, pans were hermetically sealed by crimping the pan lids upside down to minimize headspace within the sealed pans. For standard DSC runs, ramp rate of 10°C/min was used. For temperature-modulated DSC (MDSC), heat capacity was calibrated using crystalline sucrose, where the heat capacity constants were 0.988 for the direct signal and 1.049 for the reversing signal. A sinusoidal modulation of ±1°C was employed every 100 s, with a ramp rate of 2°C/min. For DSC runs, average sample weight was approximately 4–8 mg. Universal Analysis (Version 4.1D, TA Instruments) was used for DSC data analysis. Glass transition temperatures (T_g) were reported as the mid-points of the glass transition events determined from the reversing heat capacity (rev C_p) signal. Crystallization and melting temperatures were the extrapolated onset temperatures of the corresponding thermal events. Enthalpy of the exothermic events was obtained by integrating the peaks using a sigmoidal baseline. For bimodal events, enthalpy of each exotherm was obtained by drawing a perpendicular line from the valley between the two peaks onto the baseline.

Estimation of Amorphous Content

The amorphous content (ϕ) of the milled samples was quantified using Eq. (1) (26,27).

$$\phi = \frac{H_c}{H_m - \Delta C_p^{\ell-c} \times (T_m - T_c)} \times 100 \quad (1)$$

Where, H_c and H_m are the crystallization and melting enthalpies of the sample. For bimodal events, H_c was obtained by integrating both exotherms together because both exothermic peaks correspond to crystallization of glass as we will discuss later. $\Delta C_p^{l\text{-}c}$ is the difference in heat capacities of the super-cooled liquid and crystal, determined by MDSC for each material. The $\Delta C_p^{l-c} \times (T_m - T_c)$ term accounts for the effect of temperature difference between melting and crystallization events on enthalpy of crystallization. Standard DSC at 10°C/min heating rate was used to measure other parameters in Eq. (1).

Powder X-Ray Diffraction (PXRD)

A powder X-ray diffractometer (D8 Advance, Bruker AXS, Madison, WI) with CuK_α radiation and scintillation counter detector was used to examine changes in crystallinity of the samples with milling. The diffractometer was calibrated using corundum standard (SRM 674b, NIST) at d=2.0852 Å. The angular range studied was 3–35° 2θ, with step size of 0.05° and dwell time of 1 s. Milled samples were directly packed into the sample holder. Melt-quenched glasses were mildly ground using mortar and pestle before being packed for PXRD studies. All samples were packed into the sample holder by top filling method. PXRD data were collected using the Diffrac Plus XRD commander software (Bruker, AXS). Data analysis was performed using JADE (version 8, Materials Data Inc., Livermore, CA). Variable temperature XRD was conducted using a D8 Advance diffractometer, fitted with temperature-controlled stage, using a heating rate of 0.167°C/s (~10°C/min).

Particle Morphology and Surface Area

A thermally activated field emission gun type scanning electron microscope (FEG-SEM, JEOL 6500F, Tokyo, Japan) was used to characterize particle size and morphology of the milled samples. Before SEM analysis, a thin layer of platinum (thickness ~50 Å) was sputter-coated on the particle surfaces using an Ion Beam Sputter (IBS/TM200S, VCR Group Inc., CA, USA). The SEM sample chamber was maintained under a high vacuum (10^{-4} to 10^{-5} Pa) during the imaging process. Specific surface area of milled and unmilled particles was estimated by BET nitrogen gas adsorption (ASAP 2000 v3.03, Micromeritics, Norcross, Georgia).

RESULTS AND DISCUSSION

For compounds in this study, the non-isothermal crystallization of cryomilled samples is either unimodal or bimodal, while that of unmilled melt-quenched glasses is always unimodal. Table II summarizes the crystallization behaviors of milled compounds at two different milling time points, using 10°C/min DSC heating rate.

Unimodal Crystallization of Cryomilled Crystals

The crystallization behavior of γ-indomethacin glass illustrates the unimodal crystallization phenomenon (Fig. 1). Similar to a previous observation (16), the cryomilled samples show T_g comparable to its melt-quenched glass at 42–44°C, determined using 10°C/min DSC heating rate, followed by a single crystallization exotherm that corresponds to the crystallization of γ-indomethacin polymorph. The crystallization event of the milled samples, however, progressively shifts to a higher temperature with longer milling.

The up-shift in the crystallization temperature (T_c) may be attributed to the decreasing proportion of crystal seeds in milled samples with longer milling. The milled samples are verified by PXRD to be partially crystalline (data not shown). Longer duration of milling is expected to reduce the concentration of crystal seeds in the milled samples, which can explain an elevation in T_c due to slower crystallization kinetics. The

Table II Summary of Various Parameters of Eq. (1) Used to Calculate Amorphous Content (ϕ) of Milled Samples. Also Reported are the Non-Isothermal Crystallization Modes. $\Delta C_p^{l\text{-}c}$ Values are Determined from MDSC. Other Parameters are Obtained with DSC Heating Rate of 10°C/min. Standard Deviations are for Three DSC Measurements Using Independent Samples

Model API	$\Delta C_p^{l\text{-}c}$ (J/g-°C)	60 min CM				120 min CM			
		Cryst. enthalpy (J/g)	$T_m - T_c$ (°C)	ϕ (%)	Cryst. mode	Cryst. enthalpy (J/g)	$T_m - T_c$ (°C)	ϕ(%)	Cryst. mode
DPD	0.29 ± 0.02	22.6 ± 1.2	117.8 ± 2.6	71.2 ± 4.1	Unimodal	31.4 ± 1.9	105.0 ± 1.5	88.7 ± 6.0	Unimodal
KNZ	0.51 ± 0.03	36.6 ± 1.4	93.4 ± 1.8	67.3 ± 3.1	Unimodal	46.2 ± 1.1	87.0 ± 2.0	80.1 ± 2.9	Unimodal
IMC	0.47 ± 0.07	27.9 ± 1.6	94.6 ± 2.2	42.9 ± 3.1	Unimodal	42.5 ± 2.1	85.8 ± 1.4	61.4 ± 3.5	Unimodal
SMT	0.32 ± 0.02	32.2 ± 1.0	114.1 ± 2.4	41.9 ± 0.7	Unimodal	56.9 ± 2.3	108.1 ± 2.3	73.5 ± 5.5	Unimodal
TFD	0.66 ± 0.03	70.2 ± 0.9	55.8 ± 1.3	95.9 ± 2.8	Unimodal	79.6 ± 1.6	44.0 ± 3.0	98.5 ± 1.3	Unimodal
FLD	0.34 ± 0.03	21.3 ± 3.2	93.5 ± 0.9	49.8 ± 3.8	Bimodal	30.8 ± 0.6	89.0 ± 1.8	70.3 ± 1.8	Unimodal
SMZ	0.45 ± 0.05	34.3 ± 2.7	194.7 ± 2.4	56.1 ± 5.5	Bimodal	49.9 ± 2.3	190.9 ± 0.7	79.3 ± 2.4	Bimodal
PRX	0.29 ± 0.02	29.9 ± 1.9	157.1 ± 2.3	41.6 ± 2.7	Bimodal	34.6 ± 1.4	154.2 ± 1.5	47.5 ± 2.6	Bimodal
GRF	0.42 ± 0.01	30.0 ± 1.7	150.8 ± 0.8	62.7 ± 5.5	Bimodal	38.5 ± 1.3	148.2 ± 1.1	78.6 ± 3.2	Bimodal
HCT	0.32 ± 0.03	24.4 ± 2.5	163.5 ± 1.5	53.6 ± 6.2	Bimodal	37.8 ± 1.3	145.3 ± 1.0	73.7 ± 2.4	Unimodal

crystallization temperature is the highest for melt-quenched glass, which is free from detectable crystal seeds, verified by polarized light microscopy (Nikon Eclipse E200 POL, Japan). The seeding effect also explains why the cryomilled γ−polymorph sample, containing γ−polymorph seeds, always crystallizes into pure γ−polymorph, while a mixture of α (melting point ~151°C) and γ−polymorphs (melting point ~161°C) crystallize from the melt-quenched glasses where no seed for either polymorph is present. This effect of seeding on crystallization has been further supported by *ex situ* controlled seeding studies described later.

Bimodal Exotherms of Cryomilled Crystals

Five of the ten model compounds, after 60 min cryomilling, display bimodal exotherms when a 10°C/min DSC heating rate is used to heat the milled samples (Table II). The widespread occurrence of the bimodal phenomenon highlights the necessity of mechanistically understanding its physical origin. As an illustration of this behavior, the bimodal crystallization of milled piroxicam is described here. The piroxicam samples, cryomilled for different durations, show two exothermic thermal events in the total heat flow signal of standard DSC (Fig. 2a). However, for these milled samples showing bimodal behavior, T_g cannot be observed from the standard DSC traces. Instead, the first broad exothermic peak covers the temperature range where the glass transition event is expected (~60°C). However, we can readily identify glass transition of the milled piroxicam samples at ~55–59°C from the reversing signal of modulated DSC (Fig. 2b), once the contribution from the non-reversing crystallization event is separated. The T_g observed for the melt-quenched piroxicam glass is ~62–63°C by modulated DSC at 2°C/min. Similarly, T_g of milled samples can also be identified from the reversing C_p signal for other compounds that display bimodal crystallization. The observation of T_g in the milled samples suggests that they do contain amorphous domains. The partially amorphous nature of the milled piroxicam samples is further verified by PXRD overlay shown in Fig. 2c, in which both the crystalline diffraction peaks and amorphous halos are visible. There is a slight drop in T_g of the milled samples, compared to melt-quenched glass. While the exact reason for this observation is not yet clear, moisture likely does not cause it because all samples were handled in a dry environment following the same procedure. Water content was 0.39%, 0.44%, and 0.46% for samples milled for 1, 2, and 4 h respectively.

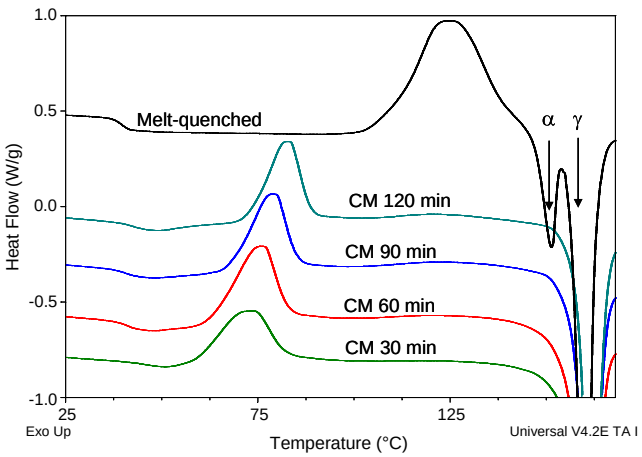

Fig. 1 Non-isothermal crystallization of cryomilled (CM) γ−indomethacin and melt-quenched indomethacin glass under standard DSC (10°C/min).

Similar to the behavior of indomethacin, the T_c of amorphous piroxicam generated through milling is significantly lower than corresponding melt-quenched glass. Similar

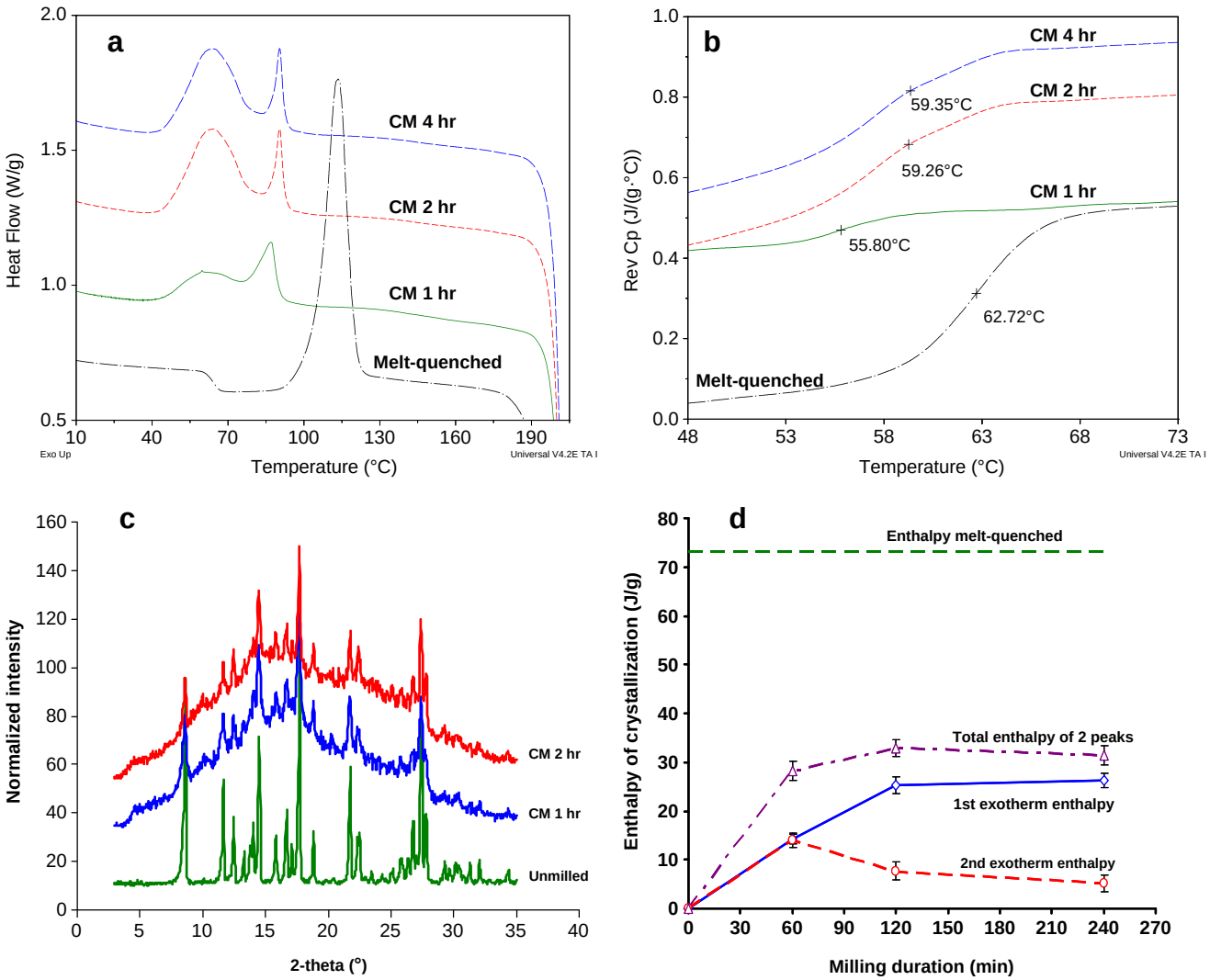

Fig. 2 Cryomilling of crystalline piroxicam polymorph I: (**a**) Characterization of cryomilled (CM) and melt-quenched piroxicam using standard DSC (heating rate 10°C/min), (**b**) reversing Cp signals by modulated DSC (heating rate 2°C/min), (**c**) PXRD patterns of milled and unmilled piroxicam, (**d**) variation of crystallization enthalpies of milled piroxicam with milling duration. Error bars represent one standard deviation of DSC measurements (n=3).

observations of depressed T_c on milling have previously been made for compounds such as sucrose (28) and dipyridamole (29). Some of the key factors causing depression in T_c of milled samples will be discussed in the later sections. Interestingly, the enthalpy of the first exothermic event increases with milling time up to 2 h, while that of the second exotherm decreases (Fig. 2d). This indicates that the physical process, responsible for the first exotherm, becomes more dominating with longer milling. However, longer milling beyond 2 h does not result in appreciable change in enthalpy ratio between the two exotherms. These changes in ratio between the two crystallization exotherms qualitatively correlate with change in particle size, which decreases with longer milling within the first two hours but is approximately constant subsequently (See supplementary information for SEM images). This observation suggests that particle size likely plays a role in bimodal crystallization phenomenon in cryomilled glasses.

A Surface Crystallization Model for Bimodal Crystallization

In examining the crystallization behaviors of different model compounds, we find that when the crystallization onset temperature of the milled samples is very close to or below bulk T_g, bimodal crystallization is always observed. On the other hand, when the T_c is well above the corresponding T_g of glasses, single crystallization exotherms are observed (Fig. 3). This definite dependence of the mode of crystallization of glass on the position of T_c relative to T_g indicates that two separate crystallization mechanisms are active below and above T_g that contribute to the two types of non-isothermal crystallization behaviors in DSC.

Faster crystallization on glass surfaces, by several orders of magnitude, compared to bulk glass, has been reported for several organic glasses at temperatures below and slightly

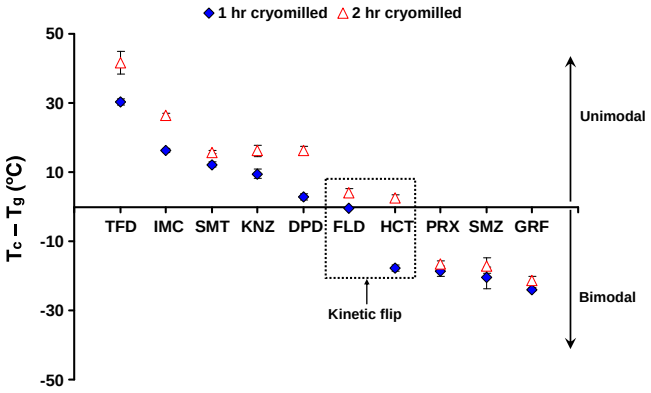

Fig. 3 Crystallization mode, unimodal or bimodal, depends on the location of T_c relative to T_g. The dotted box shows two examples where the mode of crystallization flips depending on milling duration. Data obtained at 10°C/min heating rate has been used for plotting this graph. Error bars represent one standard deviation of DSC measurements (n=3).

above T_g (30–33). This faster surface crystallization phenomenon has been explained on the basis of fast surface mobility (30,34). An alternative explanation to this phenomenon, based on density difference between the growing crystal and glass (35), was recently challenged (36). At temperatures well above T_g, surface and bulk crystallization rates of a supercooled liquid are similar due to similar molecular mobility throughout. Thus, if T_c occurs well beyond T_g, only a single crystallization exotherm is expected during DSC non-isothermal experiments. However, when the amorphous crystallization commences near or below T_g, the surface first crystallizes at a significantly faster rate, which is followed by bulk glass crystallization at higher temperatures.

The clear dependence of the mode of crystallization on T_c-T_g relationship, as shown in Fig. 3, suggests that the faster surface crystallization below T_g may be a key factor leading to the bimodal crystallization behavior of the cryomilled

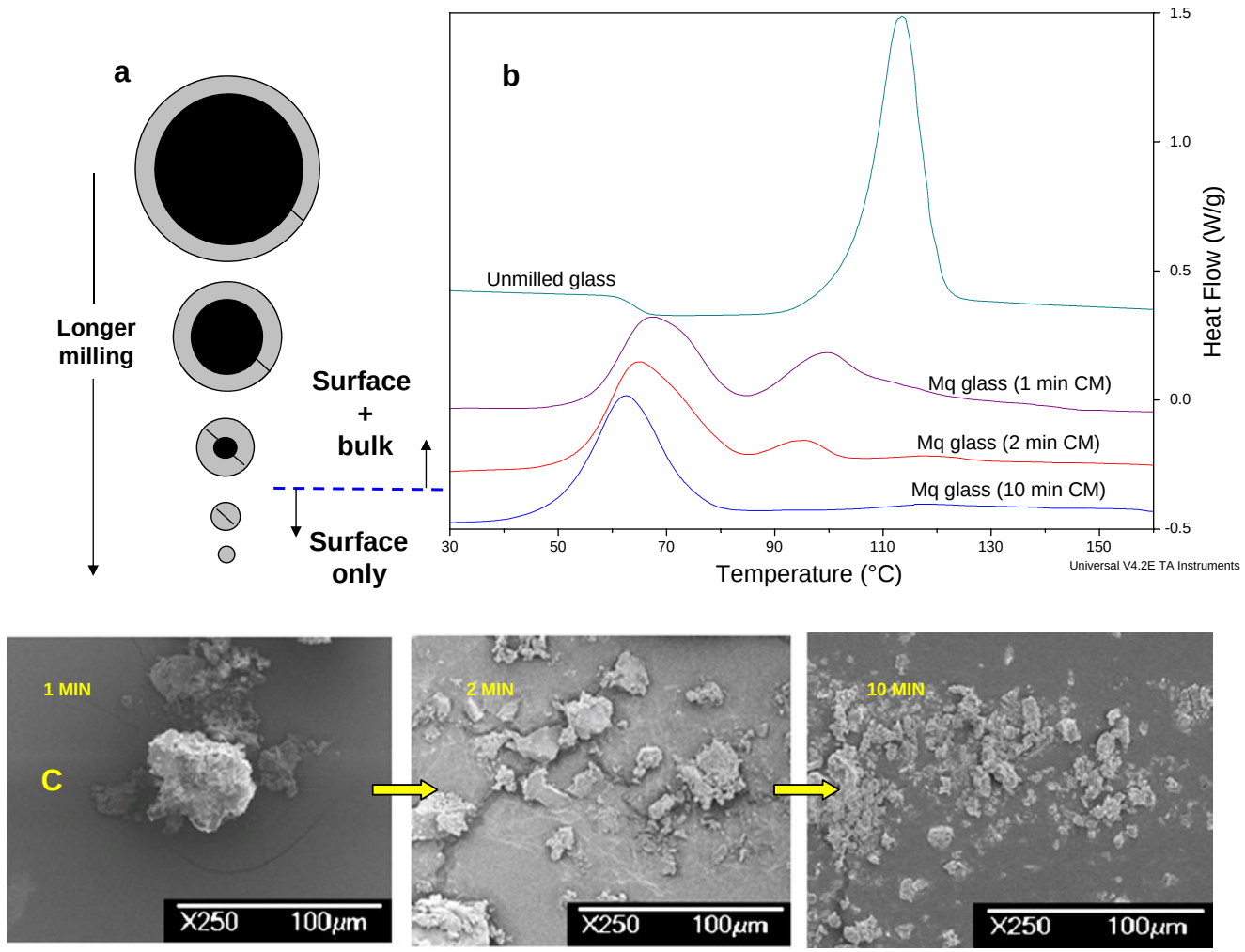

Fig. 4 (**a**) Schematic showing the relative change in proportion of surface to bulk with longer milling (**b**) DSC curves (10°C/min heating rate) for melt-quenched (Mq) piroxicam glass which was thereafter cryomilled (CM) for different durations. The crystallization exotherm shows a time dependent evolution from unimodal (unmilled glass) to bimodal (milled <10 min) and again unimodal (milled ≥10 min). (**c**) SEM images of melt-quenched piroxicam glass cryomilled for different durations.

materials. Assuming the surface layer thickness for the same glass is constant at a constant temperature below T_g, the fraction of the material in the surface layer will increase with decreasing particle size, as illustrated in Fig. 4a. For an unmilled melt-quenched glass, the percentage of fast crystallizing surface portion is negligible since the surface layer is very thin. Consequently, unmilled melt-quenched glasses display only single crystallization exotherm in DSC studies, corresponding to bulk glass crystallization at a crystallization temperature well above T_g. However, with decreasing particle size on longer milling, the fraction of the glass in the surface layer is expected to increase, corresponding to the increase in surface area as milling proceeds. For example, the specific surface area of griseofulvin is enhanced by almost ~4-fold after 1 h of milling. With increasing surface proportion, the faster surface crystallization should become more predominant and, at some point, detectable by DSC as a distinct exothermic event, followed by a second exotherm attributed to the crystallization of remaining glass. When particle size is sufficiently reduced, the second exotherm may eventually disappear as the amount of slower crystallizing bulk glass is negligible.

These expected changes in crystallization behaviors, based on the surface crystallization model, are well demonstrated with cryomilled piroxicam glass (Fig. 4b). The crystallization of the unmilled piroxicam glass (prepared by melt-quenching) is initially unimodal, but becomes bimodal when the same glass is cryomilled for 1 min. The first peak gains in enthalpy with longer milling, as particle size is reduced (Fig. 4c) while the second peak diminishes. The second peak eventually disappears after 10 min of milling. If this model is valid, it should be possible to control the mode of crystallization of a glass by controlling surface area and T_c, as discussed in the following sections.

Changing T_c of a Glass by Grinding

Reduction in particle size of glass during milling introduces more sites of heterogeneous nucleation and enhances the probability of surface crystallization, which should favor an earlier crystallization onset in milled samples compared to unmilled glass. This effect of milling on T_c of glass is demonstrated for griseofulvin glass in Fig. 5a. The crystallization onset of glass is significantly reduced with increasing milling duration. Similar observations were previously reported on indomethacin glass (37).

When the depressed T_c of the milled glass reaches the temperature of glass transition (visible only from reversing C_p signal), the crystallization mode switches from unimodal to bimodal, which may be explained by the activation of surface crystallization as discussed earlier. In Fig. 5b, the variation of enthalpies of crystallization of the two peaks with milling is shown. The total enthalpy of the bimodal crystallization of milled glasses is essentially independent of milling duration and is very close to the enthalpy of unmilled glass after correcting for the difference in crystallization onset between the unmilled and milled glasses (Fig. 5b).

Effects of Crystal Seeds and Heating Rate on T_c

In addition to particle size reduction, another factor that significantly contributes to depression in T_c of milled crystals is the presence of crystal nuclei or seeds in the milled

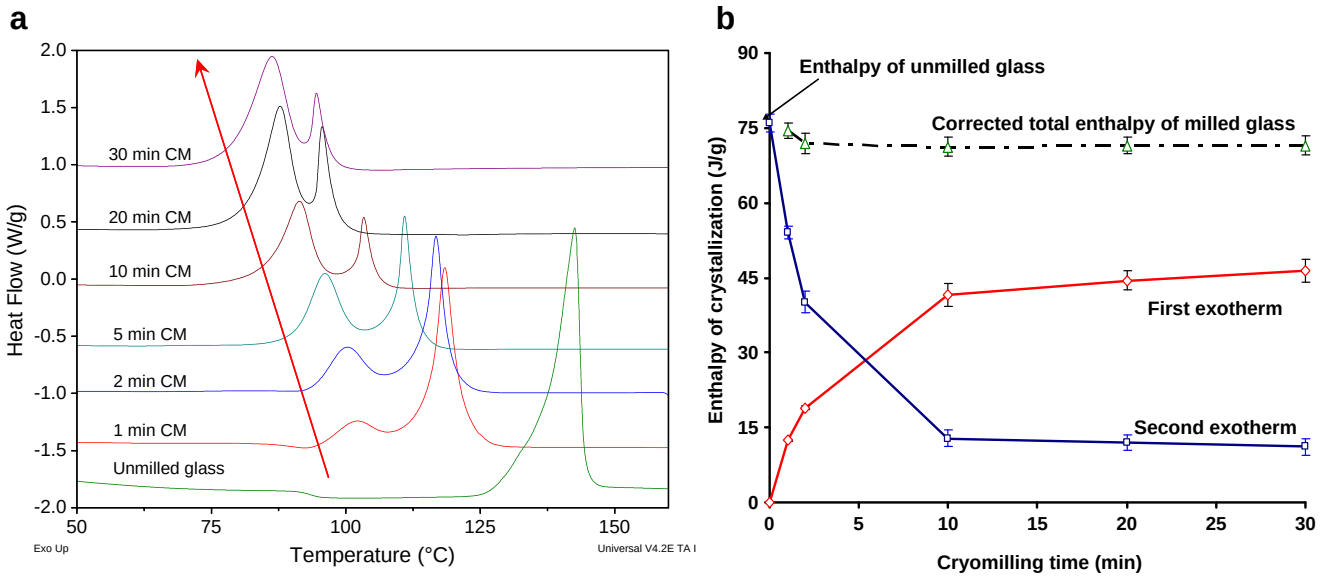

Fig. 5 Cryomilling of melt-quenched griseofulvin glass: (**a**) Effect of milling on crystallization mode of melt-quenched griseofulvin glass tested at 10°C/min heating rate. The arrow indicates that T_c is depressed with longer milling. (**b**) Dependence of crystallization enthalpies of the two exotherms on milling duration. Also plotted is the total crystallization enthalpy for the milled samples, which match closely with the crystallization enthalpy of unmilled melt-quenched glass, after performing the heat capacity corrections according to Eq. (1). Error bars represent one standard deviation of DSC measurements ($n=3$).

samples, which survive vitrification under mechanical stresses of milling. Figure 6a shows the correlation between the extent of T_c depression, ΔT_c (T_c of unmilled melt quenched glass - T_c of 1-hr cryomilled sample), and the amorphous content of milled samples for ten model compounds. Despite the scatter in the plot, there is a trend that milled materials having more seeds exhibit larger ΔT_c.

To further test the effect of seeding on T_c depression of glass, we have performed *ex situ* DSC seeding experiments by sprinkling γ−indomethacin crystal seeds on the top of melt-quenched indomethacin glass. The non-isothermal crystallization behavior of indomethacin glass at various seed concentrations of γ−indomethacin at 2°C/min heating rate are shown in Fig. 6b. At this slow heating rate, T_c of seeded indomethacin glass is lower than that observed at 10°C/min, which is expected due to the well-established effect of heating rate on crystallization onset (38). With increasing γ−indomethacin seed added, the T_c of indomethacin glasses decreases and crystallization of the γ−polymorph also becomes more predominant at the expense of α−indomethacin. This is consistent with the observations we have made in Fig. 1, where pure γ−indomethacin crystallizes from cryomilled samples that contain large proportions of γ−indomethacin crystal seeds.

The effect of T_c depression of glass by *ex situ* seeding is, however, not as drastic as observed for cryomilled materials at the same seed concentration (>45%) (Fig. 6c). For *ex situ* seeded glasses, we do not observe further depression in T_c at seed concentrations >30%. However, for milled samples, T_c

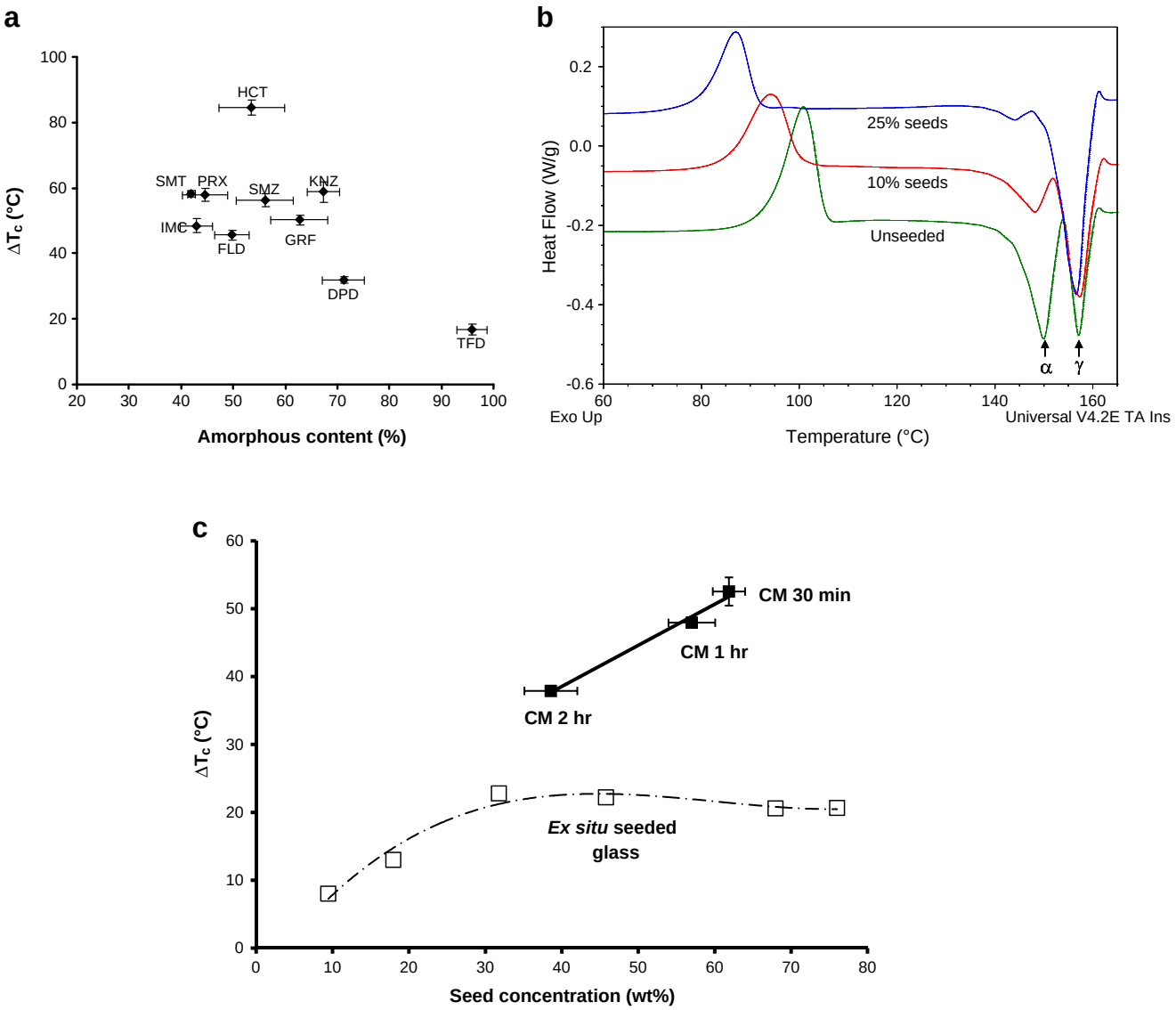

Fig. 6 (**a**) Correlation between depression in T_c of milled crystals, relative to melt-quenched glass $\left(\Delta T_c = T_c^{melt-quenched} - T_c^{1\,hr\,milled}\right)$ and amorphous content of milled samples (10°C/min heating rate). (**b**) Effect of *ex situ* seeding on crystallization onset of indomethacin glass (2°C/min heating rate). (**c**) Comparison of ΔT_c, at 10°C/min heating rate, of indomethacin cryomilled (CM) (■, n=3) with *ex situ* seeded melt-quenched glass (□, n=1).

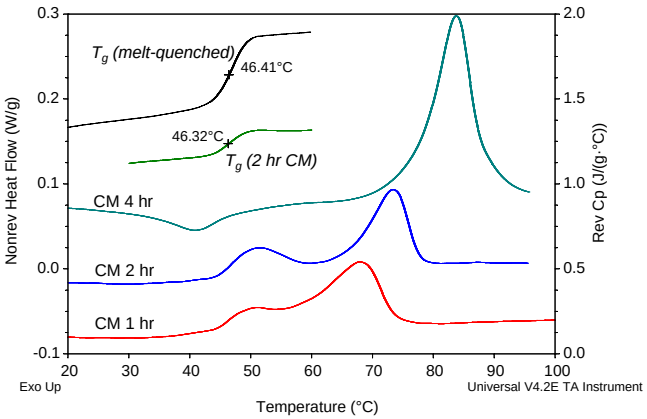

Fig. 7 Effect of milling duration on crystallization modes of cryomilled (CM) γ-indomethacin crystals tested at 2°C/min heating rate in DSC. Also shown are the T_gs of the milled and melt-quenched samples from the reversing C_p signal.

depression continues to be observed at higher seed concentrations. This is not surprising because, for *ex situ* seeded samples, the contact between crystal seeds and glass is expected to reach a maximum once a layer of crystals completely covers the glass surface. On the contrary, for cryomilled samples, crystal seeds are in intimate contact with glass throughout the sample. Therefore, T_c depression persists to a much higher seed concentration.

Kinetic Flip of Crystallization Modes

So far, we have shown that milling duration, seeding, and heating rate can all affect T_c of a glass. If T_c of a cryomilled sample can be kinetically controlled through these parameters to be either below or above T_g, we should observe flip between the unimodal and bimodal crystallization behaviors for the same glass if the surface crystallization model is valid.

In fact, we do observe kinetic flip between unimodal and bimodal crystallization by modifying milling duration. For example, T_c of the indomethacin crystals milled for 2 h at 2°C/min heating rate (~43°C) is slightly lower than its T_g (~46°C determined from reversing C_p) and bimodal crystallization occurs (Fig. 7). At the same heating rate, however, T_c of indomethacin after 4 h of cryomilling (76°C) is 30°C beyond T_g and only a single crystallization peak is observed (Fig. 7).

Similar milling-induced flipping behavior can also be observed for felodipine and hydrochlorothiazide. Provided faster surface crystallization is universal, our model predicts that any organic glass can display either crystallization behaviors depending on kinetics of crystallization. When felodipine crystals are milled for 1 h, the T_c (46°C) is approximately the same as T_g (~46.2°C) and bimodal crystallization behavior is observed (Fig. 8a). However, longer milling duration (4 h) shifts the crystallization onset to a temperature (66°C) much higher than its T_g. Consequently, only a single crystallization peak is observed (Fig. 8a).

At a heating rate of 10°C/min, the T_c of the 2 h milled felodipine (51°C) is ~5°C higher than T_g (~46°C). For this sample, a small leading shoulder can still be observed before the main crystallization event (Fig. 8a), indicating faster surface crystallization remains active at slightly above T_g. This is consistent with the observation that the faster surface crystallization process remains active up to a few degrees above T_g instead of being abruptly turned off at T_g (30). However, when the same 2 h milled felodipine sample is heated at a slower heating rate at 2°C/min during the MDSC experiments, the T_c (46°C) is below its T_g (~47.2°C determined at 2°C/min from reversing C_p) and we observe a

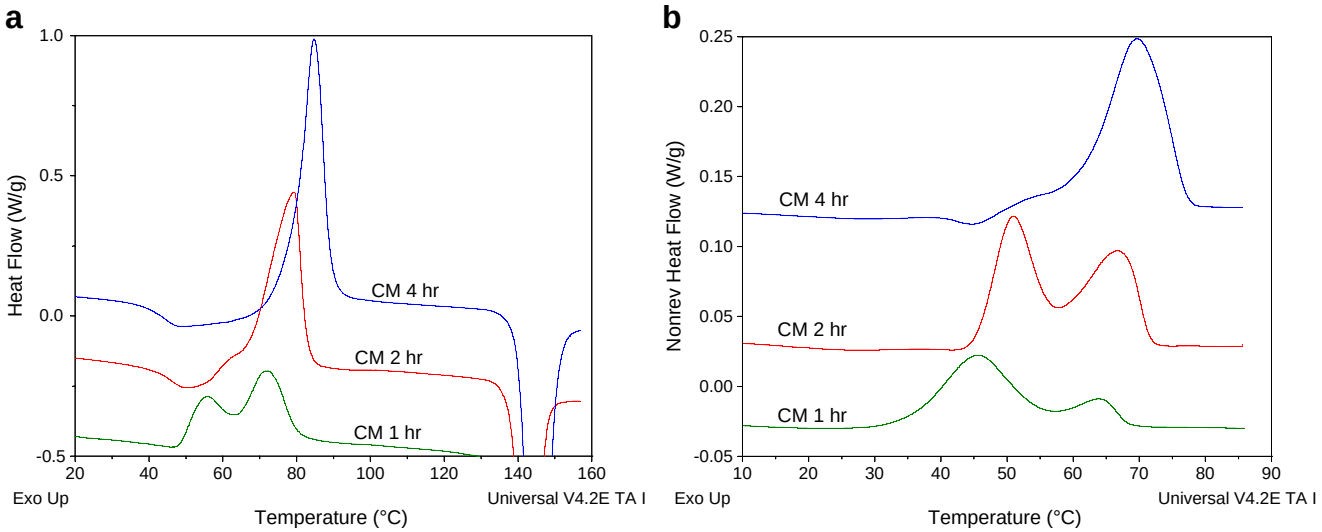

Fig. 8 Non-isothermal crystallization of cryomilled (CM) felodipine crystals, showing flip between unimodal and bimodal crystallization under (**a**) standard DSC (10°C/min), and (**b**) modulated DSC (non-reversing heat flow, 2°C/min).

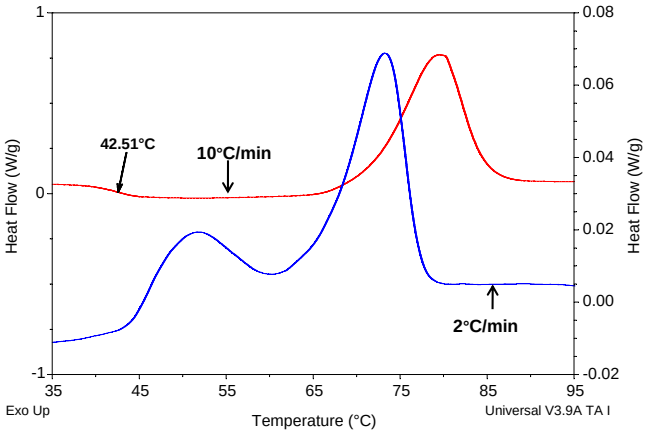

Fig. 9 Effect of heating rate on the crystallization behaviors of crystalline indomethacin cryomilled for 2 h. Crystallization is unimodal at 10°C/min but bimodal at 2°C/min for the same glass prepared by 2 h milling, due to faster crystallization onset at slower heating rate.

clear bimodal crystallization behavior (Fig. 8b). The heating rate-induced kinetic flip in crystallization mode for the same sample effectively excludes the possibility that the bimodal thermal behavior is simply a consequence of the presence of two size populations of particles in the cryomilled samples. Such an explanation cannot explain the unimodal crystallization behavior of some cryomilled samples anyway.

Similar to felodipine, heating rate-induced flipping in crystallization mode is also observed for indomethacin. Indomethacin, cryomilled for 2 h, shows unimodal crystallization behavior (T_c of 71°C and T_g of ~44°C), when tested at a heating rate of 10°C/min in DSC. However, the same sample shows bimodal crystallization when a slower heating rate of 2°C/min is used (T_c of 42.9°C and T_g of ~46°C from reversing C_p) (Fig. 9).

For some materials, an increase in heating rate from 2°C/min to 10°C/min does not cause a sufficient change in T_c to switch from bimodal crystallization to unimodal behavior. However, the relative sizes of the two crystallization exotherms in the bimodal event vary according to the proposed surface crystallization model. For instance, when a sample of crystalline piroxicam, cryomilled for 2 h, is subjected to a slower heating rate of 2°C/min during modulated DSC experiments, the ratio of the area of the first crystallization peak to that of the second peak is 26:1. However, at a faster heating rate of 10°C/min, the ratio reduces to 4.4:1 for the same sample. This is expected because more time is available for the surface to crystallize completely at a slower heating rate, which increases the first exotherm area at the expense of the second exotherm.

Flip Induced by Polymer

The phenomenon of kinetic flipping between unimodal and bimodal behaviors by simply changing the heating rate or milling duration supports the surface crystallization model, which well explains the two crystallization behaviors. The validity of this model can also be further tested if we can flip the crystallization from bimodal to unimodal, by raising the T_c to above T_g of a glass using crystallization inhibitors. To test this, crystalline griseofulvin was cryomilled for 30 min in presence of crystallization inhibitor polyvinyl pyrrolidone vinyl acetate (PVPVA, Kollidon VA 64 Fine, BASF Corporation). Milling of griseofulvin alone for 30 min yields an amorphous phase that exhibits bimodal crystallization, with T_c approximately 25°C below T_g (90°C). The presence of polymer slows down the crystallization and hence elevates T_c as expected but does not affect T_g of griseofulvin (~90°C), as seen from the reversing C_p signal in Fig. 10. This is likely because griseofulvin does not form strong hydrogen bond interactions with PVPVA, since both do not have strong hydrogen bond donors.

When cryomilled with 20% PVPVA, the T_c of griseofulvin almost coincides with T_g of griseofulvin and the bimodal peaks

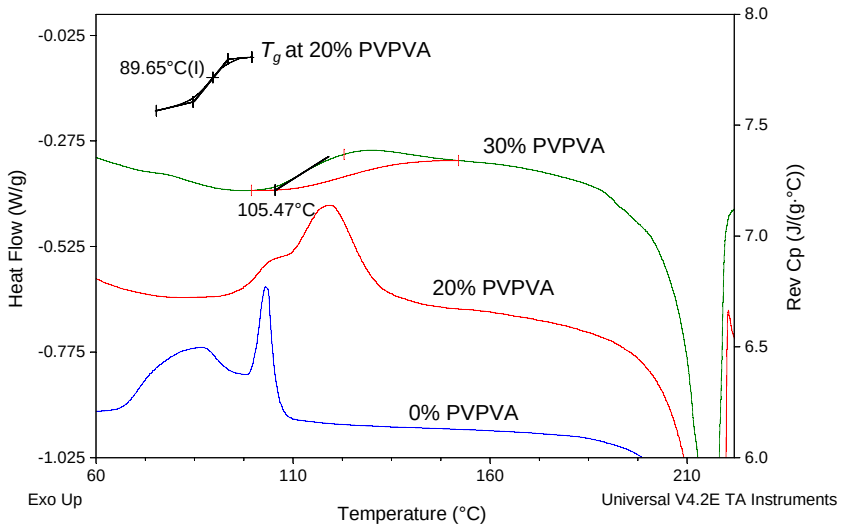

Fig. 10 Effect of polymer on crystallization onset and mode of crystallization of 30 min cryomilled griseofulvin. Also shown is the reversing C_p signal for 20% PVPVA loading that confirms that T_g of griseofulvin (~90°C) is unchanged in presence of the polymer.

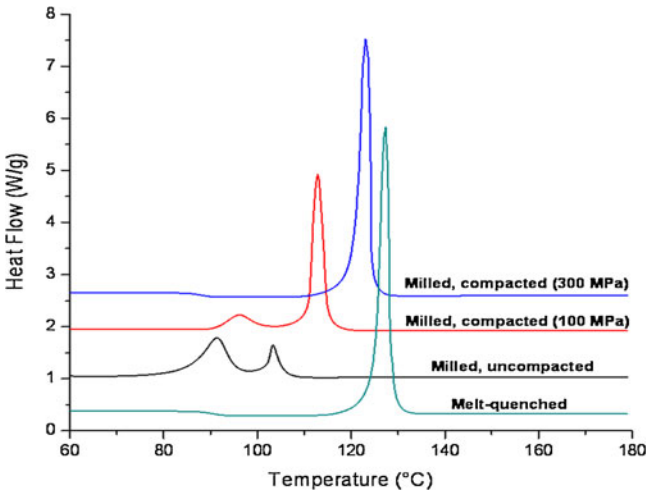

Fig. 11 Effect of compaction on crystallization behavior of griseofulvin glass (prepared by melt-quenching followed by cryomilled for 10 min). For uncompacted cryomilled glass, crystallization is clearly bimodal, with surface proportion (*i.e.*, the first exotherm) accounting for ~70% of total enthalpy. After compaction at 100 MPa pressure, the surface proportion accounts for ~24% of overall crystallization. With 300 MPa pressure, the first exotherm (surface) is eliminated and the crystallization is unimodal at $T>T_g$.

begin to merge into a single exotherm. When the T_c (~106°C) is well beyond T_g (~90°C) at 30% PVPVA loading, only unimodal crystallization behavior is observed. This experiment further supports that the bimodal exothermic event is caused by faster surface crystallization.

Flip Induced by Surface Elimination

We have shown that size reduction of glasses can induce bimodal crystallization (Fig. 5a). An excellent further test of our model is to convert bimodal crystallization to unimodal by eliminating surface area that was originally generated by milling. Cryomilled griseofulvin glass was compressed into thin discs (4 mm diameter) at the pressures of 100 and 300 MPa. It is expected that consolidation of a powder diminishes powder porosity, hence, total surface area (39,40). We therefore expect reduced size of the first exotherm, which is attributed to surface crystallization, after compaction. As-milled griseofulvin glass displays clear bimodal crystallization, with the first exotherm accounting for ~70% of the total enthalpy (Fig. 11). For the disc compressed at 100 MPa, surface proportion accounts for ~24% of overall crystallization. With 300 MPa pressure, the surface crystallization peak is eliminated (Fig. 11), and crystallization behavior resembles that of the unmilled melt-quenched glass. The total enthalpy of crystallization (after correction for the effect of Tc difference on enthalpy of crystallization), for milled and compacted samples, match closely with that of melt-quenched glass that has not been subjected to any mechanical stress. This experiment confirms that surface crystallization of milled samples is indeed responsible for the first exothermic event in bimodal crystallization, which can be eliminated by compaction.

Possibility of Crystallization into Different Polymorphs

Crystallization into two distinct polymorphs can result in bimodal crystallization, when crystallization onset is higher than T_g for some organic glasses (24,25). However, the possibility of different polymorphs crystallizing can be ruled out for molecules, such as griseofulvin, which exhibit bimodal crystallization behavior despite having no known polymorphs. Figure 12a shows that only a single crystalline phase crystallizes during the entire process of crystallization of cryomilled griseofulvin over a temperature range covering both exotherms. In the temperature range of the bimodal events (10°C/min was

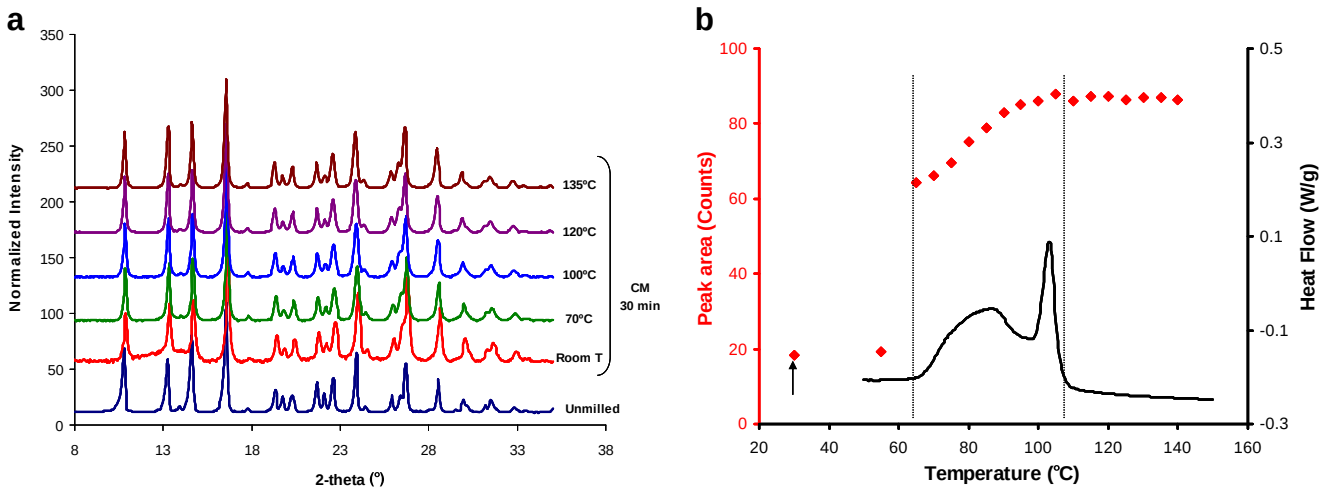

Fig. 12 (**a**) Overlay of variable temperature XRD and (**b**) integrated area of X-ray diffraction peak at 16.6° 2θ as a function of temperature, along with the DSC trace showing the bimodal behavior, for 30 min cryomilled griseofulvin. The arrow indicates the room temperature X-ray peak area for the milled sample.

used for both VTPXRD and DSC experiments), we only observe a progressive increase in fraction of the same crystalline form of griseofulvin, estimated by integrating the area of peak maxima at 16.6° 2θ (Fig. 12b). Both exothermic events, therefore, correspond to crystallization of the amorphous phase into the same crystal form. Moreover, all model compounds that exhibit bimodal crystallization in this work have only a single melting endotherm following crystallization during DSC experiments. Thus, the possibility of bimodal events corresponding to crystallization of different polymorphs may be excluded for these compounds. It is possible that a polymorphic transition may be exothermal. If so, two exotherms may be observed for a glass that undergoes unimodal crystallization. However, the two exotherms (crystallization of the glass and polymorphic transition) are usually well separated. It is also possible that a glass may crystallize into two polymorphs at different temperatures. In both cases, crystallization events take place at temperatures above T_g and can be readily distinguished from the bimodal crystallization phenomenon discussed in this report.

CONCLUSIONS

In this work, we have described a surface crystallization model that can be used to explain both unimodal and bimodal crystallization of organic glasses prepared by different routes. We have shown that the modes of crystallization of all molecules in this study are determined by the position of crystallization onset, T_c, relative to glass transition temperatures, T_g. Unimodal crystallization occurs when T_c is at least several degrees higher than T_g. Bimodal crystallization takes place when T_c is lower than or close to T_g. This model clearly explains the otherwise perplexing effects of milling duration, heating rate, particle size, crystallization inhibition, and compaction on the thermal behavior of organic glasses.

ACKNOWLEDGMENTS & DISCLOSURES

We thank Boehringer-Ingelheim Pharmaceuticals Inc, Ridgefield, CT for financial support to this work. Some of the experiments were performed at the University of Minnesota I.T. Characterization Facility, which receives partial support from the NSF through the NNIN program.

REFERENCES

1. Yu L. Amorphous pharmaceutical solids: preparation, characterization and stabilization. Adv Drug Del Rev. 2001;48:27–42.
2. Hilden LR, Morris KR. Physics of amorphous solids. J Pharm Sci. 2001;93:3–12.
3. Levine H, Slade L, Levine H. Progress in food processing and storage, based on amorphous product technology. Cambridge: The Royal Society of Chemistry; 2002.
4. Blanshard JMV, Lillford P. The glassy state in foods. Nottingham: Nottingham University Press; 1993.
5. Crowe JH, Carpenter JF, Crowe LM. The role of vitrification in anhydrobiosis. Annu Rev Physiol. 1998;60:73–103.
6. Greer AL. Metallic glasses. Science. 1995;267:1947–53.
7. Fan GJ, Guo FQ, Hu ZQ, Quan MX, Lu K. Amorphization of selenium induced by high-energy ball milling. Phys Rev B. 1997;55:11010–3.
8. Lin ZJ, Zhuo MJ, Sun ZQ, Veyssiere P, Zhou YC. Amorphization by dislocation accumulation in shear bands. Acta Mater. 2009;57:2851–7.
9. Huttenrauch R, Fricke S, Zeilke P. Mechanical activation of pharmaceutical systems. Pharm Res. 1985:302–306.
10. Willart JF, Descamps M. Solid state amorphization of pharmaceuticals. Mol Pharm. 2008;5:905–20.
11. Willart JF, De Gusseme A, Hemon S, Odou G, Danede F, Descamps M. Direct crystal to glass transformation of trehalose induced by ball milling. Solid State Comm. 2001;119:501–5.
12. Suryanarayana C. Mechanical alloying and milling. Progr Mater Sci. 2001;46:1.
13. Tromans D, Meech JA. Enhanced dissolution of minerals: Stored energy, amorphism and mechanical activation. Miner Eng. 2001;14:1359–77.
14. Liu J, Rigsbee DR, Stotz C, Pikal MJ. Dynamics of pharmaceutical amorphous solids: the study of enthalpy relaxation by isothermal microcalorimetry. J Pharm Sci. 2002;91:1853–62.
15. Hodge IM. Enthalpy relaxation and recovery in amorphous materials. J Non-Cryst Solids. 1994;169:211–66.
16. Crowley KJ, Zografi G. Polymorphs and solvates: assessment of amorphous phase formation and amorphous phase physical stability. J Pharm Sci. 2002;91:492–507.
17. Bhugra C, Rambhatla S, Bakri A, Duddu SP, Miller DP, Pikal MJ, Lechuga-Ballesteros D. Prediction of the onset of crystallization of amorphous sucrose below the calorimetric glass transition temperature from correlations with mobility. J Pharm Sci. 2007;96:1258–69.
18. Bhugra C, Pikal MJ. role of thermodynamic, molecular, and kinetic factors in crystallization from the amorphous state. J Pharm Sci. 2008;97:1329–49.
19. Roberts CJ, Debenedetti PG. Engineering pharmaceutical stability with amorphous solids. AIChE J. 2002;48:1140–4.
20. Feng T, Pinal R, Carvajal MT. Process induced disorder in crystalline materials: differentiating defective crystals from the amorphous form of griseofulvin. J Pharm Sci. 2008;97:3207–21.
21. Feng T, Bates S, Carvajal MT. Toward understanding the evolution of griseofulvin crystal structure to a mesophase after cryogenic milling. Int J Pharm. 2008;367:16–9.
22. Chamarthy SP, Pinal R. The nature of crystal disorder in milled pharmaceutical materials. Colloid Surface A. 2008;331:68–75.
23. Trasi NS, Boerrigter SXM, Byrn SR. Investigation of the milling-induced thermal behavior of crystalline and amorphous griseofulvin. Pharm Res. 2010;27:1377–89.
24. Yu L, Mishra D, Rigsbee DR. Determination of glass properties of mannitol using sorbitol as an impurity. J Pharm Sci. 1998;87:774–7.
25. Zhou D, Schmitt EA, Zhang GG, Law D, Vyazovkin S, Wright CA, Grant DJW. Crystallization kinetics of amorphous nifedipine studied by model-fitting and model-free approaches. J Pharm Sci. 2003;92:1779–92.
26. Lefort R, De Gusseme A, Willart JF, Danede F, Descamps M. Solid state NMR and DSC methods for quantifying the amorphous content in solid dosage forms: an application to ball-milling of trehalose. Int J Pharm. 2004;280:209–19.
27. Grisedale LC, Jamieson MJ, Belton PS, Barker SA, Craig DQM. Characterization and quantification of amorphous material in milled and spray-dried salbutamol sulfate: a comparison of thermal,

spectroscopic, and water vapor sorption approaches. J Pharm Sci. 2011;100:3114–29.
28. Saleki-Gerhardt A, Ahlneck C, Zografi G. Assessment of disorder in crystalline solids. Int J Pharm. 1994;101:237–47.
29. Patterson JE, James MB, Forster AH, Lancaster RW, Butler JM, Rades T. The influence of thermal and mechanical preparative techniques on the amorphous state of four poorly soluble compounds. J Pharm Sci. 2005;94:1998–2012.
30. Wu T, Yu L. Surface crystallization of indomethacin below T_g. Pharm Res. 2006;23:2350–5.
31. Zhu L, Jona J, Nagapudi K, Wu T. Fast surface crystallization of amorphous griseofulvin below T_g. Pharm Res. 2010;27:1558–67.
32. Zhu L, Wong L, Yu L. Surface-enhanced crystallization of amorphous nifedipine. Mol Pharm. 2008;5:921–6.
33. Sun Y, Zhu L, Kearns KL, Ediger MD, Yu L. Glasses crystallize rapidly at free surfaces by growing crystals upward. Proc Natl Acad Sci U S A. 2011;108:5990–5.
34. Zhu L, Brian CW, Swallen SF, Straus PT, Ediger MD, Yu L. Surface self-diffusion of an organic glass. Phys Rev Lett. 2011;106:256103-1–4.
35. Schmelzer J, Pascova R, Moller J, Gutzow I. Surface-induced devitrification of glasses: the influence of elastic strains. J Non-Cryst Solids. 1993;162:26–39.
36. Gunn EM, Guzei IA, Yu L. Does crystal density control fast surface crystal growth in glasses? A study with polymorphs. Cryst Growth Des. 2011;11:3979–84.
37. Bhugra C, Shmeis R, Pikal MJ. Role of mechanical stress in crystallization and relaxation behavior of amorphous indomethacin. J Pharm Sci. 2007;97:4446–58.
38. Ozawa T. Critical investigation of methods for kinetic analysis of thermoanalytical data. J Therm Anal. 1975;7:601–17.
39. Sun CC, Grant DJW. Compaction properties of L-lysine salts. Pharm Res. 2001;18:281–6.
40. Sun CC. Mechanism of moisture induced variations in true density and compaction properties of microcrystalline cellulose. Int J Pharm. 2008;346:93–101.